










# Stellar and Molecular Gas Rotation in a Recently Quenched Massive Galaxy at $z \sim 0.7$

Qiana Hunt<sup>1</sup>, Rachel Bezanson<sup>2</sup>, Jenny E. Greene<sup>1</sup>, Justin S. Spilker<sup>3</sup> , Katherine A. Suess<sup>4</sup> , Mariska Kriek<sup>4</sup> ,  
Desika Narayanan<sup>5,6,7</sup> , Robert Feldmann<sup>8</sup> , Arjen van der Wel<sup>9,10</sup> , and Petchara Pattarakijwanich<sup>11</sup> 

<sup>1</sup> Department of Astrophysics, Princeton University, Princeton, NJ 08544, USA

<sup>2</sup> Department of Physics and Astronomy and PITT PACC, University of Pittsburgh, Pittsburgh, PA 15260, USA

<sup>3</sup> Department of Astronomy, University of Texas at Austin, 2515 Speedway, Stop C1400, Austin, TX 78712, USA

<sup>4</sup> Astronomy Department, University of California, Berkeley, CA 94720, USA

<sup>5</sup> Department of Astronomy, University of Florida, 211 Bryant Space Sciences Center, Gainesville, FL 32611, USA

<sup>6</sup> University of Florida Informatics Institute, 432 Newell Drive, Gainesville, FL 32511, USA

<sup>7</sup> Cosmic Dawn Center (DAWN), Niels Bohr Institute, University of Copenhagen, Juliane Maries vej 30, DK-2100 Copenhagen, Denmark

<sup>8</sup> Institute for Computational Science, University of Zurich, CH-8057 Zurich, Switzerland

<sup>9</sup> Sterrenkundig Observatorium, Universiteit Gent, Krijgslaan 281 S9, B-9000 Gent, Belgium

<sup>10</sup> Max-Planck Institut für Astronomie, Königstuhl 17, D-69117, Heidelberg, Germany

<sup>11</sup> Department of Physics, Faculty of Science, Mahidol University, Bangkok 10400, Thailand

Received 2018 March 30; revised 2018 June 4; accepted 2018 June 4; published 2018 June 18

## Abstract

The process by which massive galaxies transition from blue, star-forming disks into red, quiescent galaxies remains one of the most poorly understood aspects of galaxy evolution. In this investigation, we attempt to gain a better understanding of how star formation is quenched by focusing on a massive post-starburst galaxy at  $z = 0.747$ . The target has a high stellar mass and a molecular gas fraction of 30%—unusually high for its low star formation rate (SFR). We look for indicators of star formation suppression mechanisms in the stellar kinematics and age distribution of the galaxy obtained from spatially resolved Gemini Integral-field spectra and in the gas kinematics obtained from the Atacama Large Millimeter/submillimeter Array (ALMA). We find evidence of significant rotation in the stars, but we do not detect a stellar age gradient within 5 kpc. The molecular gas is aligned with the stellar component, and we see no evidence of strong gas outflows. Our target may represent the product of a merger-induced starburst or of morphological quenching; however, our results are not completely consistent with any of the prominent quenching models.

*Key words:* galaxies: evolution – galaxies: formation – galaxies: kinematics and dynamics

## 1. Introduction

Luminous galaxies in the low- and intermediate-redshift universe can generally be divided into two distinct populations: blue active spirals; and red quiescent ellipticals (e.g., Strateva et al. 2001; Alatalo et al. 2014). Red galaxies, which harbor little or no star formation, must have formed their stars at some point in the early universe and thus are the descendants of once-active blue galaxies (e.g., Bell et al. 2004; Faber et al. 2007). The transition from one stage to the other requires the suppression, or quenching, of star formation. Little is known about the specific processes responsible for quenching massive galaxies. Recent studies suggest a strong correlation between structural changes in the galaxy and star formation suppression (e.g., Newman et al. 2015; Yano et al. 2016). Several models have been proposed. For instance, *gas-poor mergers* may suppress star formation by heating the surrounding gas halo via inflow-triggered shocks (Hopkins et al. 2009; Johansson et al. 2009; Naab et al. 2009). *Gas-rich major mergers* may also heat up the gas supply and guard it against gravitational collapse (Hopkins et al. 2008), or disrupt the cold gas disk. Mergers may lead to *compaction*, in which the star-forming gas migrates inward, triggering a central starburst and inside-out gas depletion (Tacchella et al. 2015; Wellons et al. 2015; Zolotov et al. 2015), or can trigger high-velocity *outflows* driven by starburst radiation or quasar activity (Tremonti et al. 2007; Sell et al. 2014; Pontzen et al. 2017; Mao & Ostriker 2018). Alternatively, galaxies may quench without removing cold gas if the gas is stabilized against clumping by dynamical effects following *gas-rich minor mergers*

(van de Voort et al. 2018) or *morphological quenching* (Martig et al. 2009).

Different quenching scenarios should leave characteristic marks on the distribution of ages and motions of stars within quiescent galaxies. However, these signatures gradually diminish over time (Cananzi et al. 1993; Goto et al. 2003; Kauffmann et al. 2003). In order to better understand the quenching process, it is necessary to observe galaxies soon after they transition. Post-starburst galaxies (PSBs)—galaxies that suddenly turned quiescent after a period of intense star formation—are ideal subjects. Their spectra are dominated by A-type stars with lifespans on the order of  $\sim 1$  Gyr (e.g., Poggianti & Barbaro 1997; Le Borgne et al. 2006), so a lack of current star formation suggests that they must have quenched within a few Gyr before observation. As “transitional objects,” PSBs may represent a bridge between massive blue and red galaxies (e.g., Alatalo et al. 2014).

In this Letter, we examine an intermediate-redshift PSB, SDSS J0912+1523, with a stellar mass of  $\sim 2 \times 10^{11} M_{\odot}$ . The target was chosen out of a large sample of PSBs (Suess et al. 2017) selected from the Sloan Digital Sky Survey (SDSS) DR12 catalog (Alam et al. 2015) and included in Pattarakijwanich et al. (2016). The galaxies in the PSB sample were identified by their strong Balmer breaks and blue slopes redward of the break, as demonstrated in Kriek et al. (2010). SDSS J0912+1523 was chosen as the brightest, most A-star dominated source at the high end of the sample’s redshift range, with  $z = 0.747$  and  $i_{AB} = 18.6$  mag. SDSS J0912+1523 represents a rare opportunity to study the spatially resolved

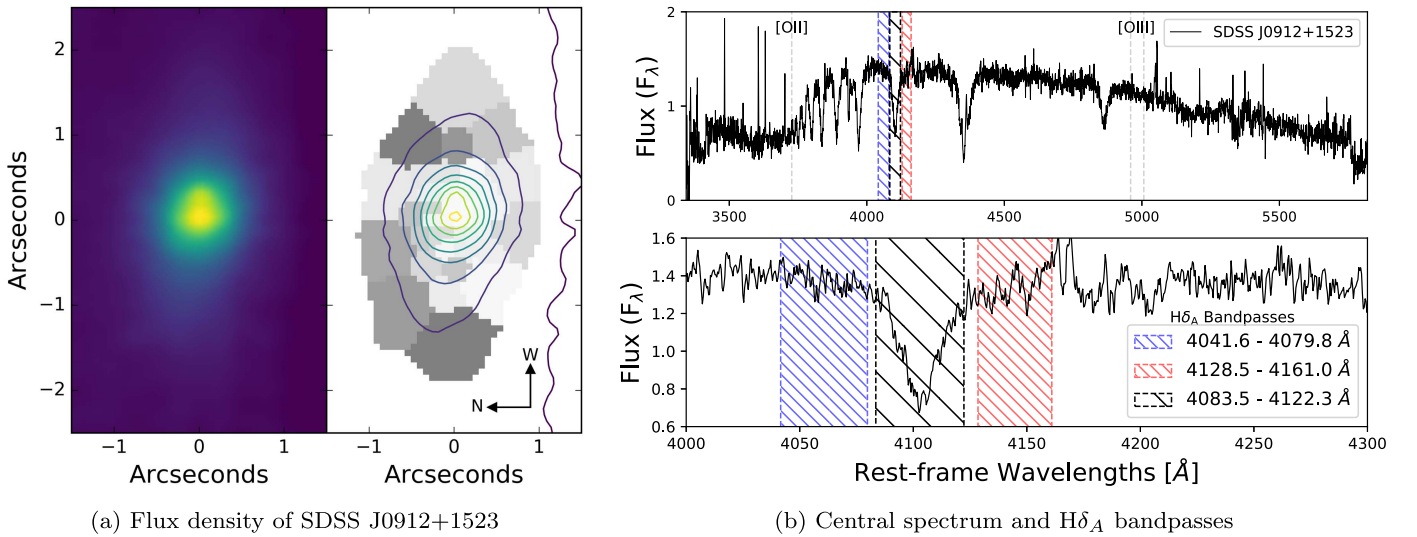


**Figure 1.** (a) Median flux map of SDSS J0912+1523 from the Gemini spectra, with contours overlaid onto the Voronoi bins. (b) Full spectrum of the central Voronoi bin and the  $H\delta_A$  central bandpass, surrounded by blue and red “continuum” bandpasses, as defined by Worthey & Ottaviani (1997). The wavelengths of the [O II] $\lambda$ 3727, [O III] $\lambda$ 4959, and [O III] $\lambda$ 5007 lines are labeled.

kinematics of a massive, recently quenched PSB. Suess et al. (2017) presented Atacama Large Millimeter/submillimeter Array (ALMA) observations of the galaxy’s molecular gas. Here, we analyze the stellar component observed by Gemini to obtain the kinematic properties and age distribution of the stellar population. Combining the stellar and gas data, we identify markers left by the quenching process and constrain the means by which SDSS J0912+1523 suppressed its star formation. We assume a cosmology of  $\Omega_m = 0.3$ ,  $\Omega_\Lambda = 0.7$ , and  $h = 0.7$ .

## 2. Data

We obtained a spatially resolved spectral datacube from observations of SDSS J0912+1523 made with the Gemini North 8 m telescope in 2016 March. The target was observed using GMOS-N in one-slit IFU mode with the R400 grating, giving a field of view of approximately  $7'' \times 5''$ . We acquired five exposures of 24.5 minutes each. The observations have a spectral FWHM of  $\sim 1.35 \text{ \AA}$  under  $\sim 0''.5$  seeing conditions, as reported by the Gemini staff. Our data yield spectral coverage over 3343–5820  $\text{\AA}$  in the rest frame. We reduced the data with `gemtools` and `gmos` in the Gemini IRAF package<sup>12</sup> using the procedure described by Lena (2014).

We collapse our datacube in the spectral dimension by taking the median flux of each spaxel. The resulting 2D flux distribution and contour maps are shown in Figure 1(a). We note an asymmetry in the object’s core, which may indicate the presence of two peaks. The flux of the secondary peak,  $\sim 0''.2$  west of the galaxy’s center, reaches 91% of the maximum. We investigate the nature of the peaks in Section 3.

We remove all spaxels with individual signal-to-noise ratios (S/N) beneath a threshold of 0.3 from the flux map and spatially bin the remainder using an adaptive Voronoi method (Cappellari & Copin 2003). We set the target S/N of the spatial bins to 6. The median galaxy spectrum of the spaxels in each bin is then calculated and examined individually.

<sup>12</sup> <http://www.gemini.edu/sciops/instruments/gmos/>

### 2.1. Spatially Resolved Kinematics

The Penalized Pixel-Fitting (pPXF) software (Cappellari & Emsellem 2004; Cappellari 2017) is used to extract stellar kinematics from each Voronoi bin by fitting a set of higher-resolution template spectra to the galaxy spectrum. We use theoretical simple stellar population model templates with a resolution of  $R = 10,000$  created by Charlie Conroy (R. Bezanson et al. 2018, in preparation). We assume solar metallicity and mask the strong telluric features in the galaxy spectrum. The template and median spectra are fed into pPXF, which convolves the templates to the observed spectral resolution and fits a non-negative combination of the templates to the spectrum, along with a multiplicative and additive polynomial that accounts for dust reddening in addition to potential issues with flux calibration. The code returns a best-fitting stellar population model, stellar velocity, and velocity dispersion (hereafter referred to as  $\sigma$ ). Maps of velocity and  $\sigma$  are shown in Figures 2(b) and (c).

The uncertainties in velocity and  $\sigma$  are derived using 100 iterations of Monte Carlo resampling, in which the residuals are randomly sampled, added to the best-fitting model, and rerun through pPXF as the new “galaxy” spectrum. The typical uncertainty is  $22 \text{ km s}^{-1}$  for stellar velocity and  $10 \text{ km s}^{-1}$  for  $\sigma$ .

### 2.2. Measuring Age-sensitive Spectral Indices

The hydrogen Balmer lines are strong absorption features that dominate the spectra of A-type stars. Because they are sensitive to emission-filling by ongoing star formation, the strong presence of these features in the absence of emission lines indicates a burst of star formation followed by sudden suppression and passive evolution (e.g., Cananzi et al. 1993; Goto et al. 2003; Kauffmann et al. 2003). For PSB populations, stronger Balmer absorption features signify more recent bursts (Kauffmann et al. 2003).

We use the equivalent width (EW) of the  $H\delta$  Balmer line as a proxy for stellar ages.  $H\delta$  is well isolated from other spectral features and less susceptible to contamination from emission-filling than other Balmer lines (Goto et al. 2003). We measure

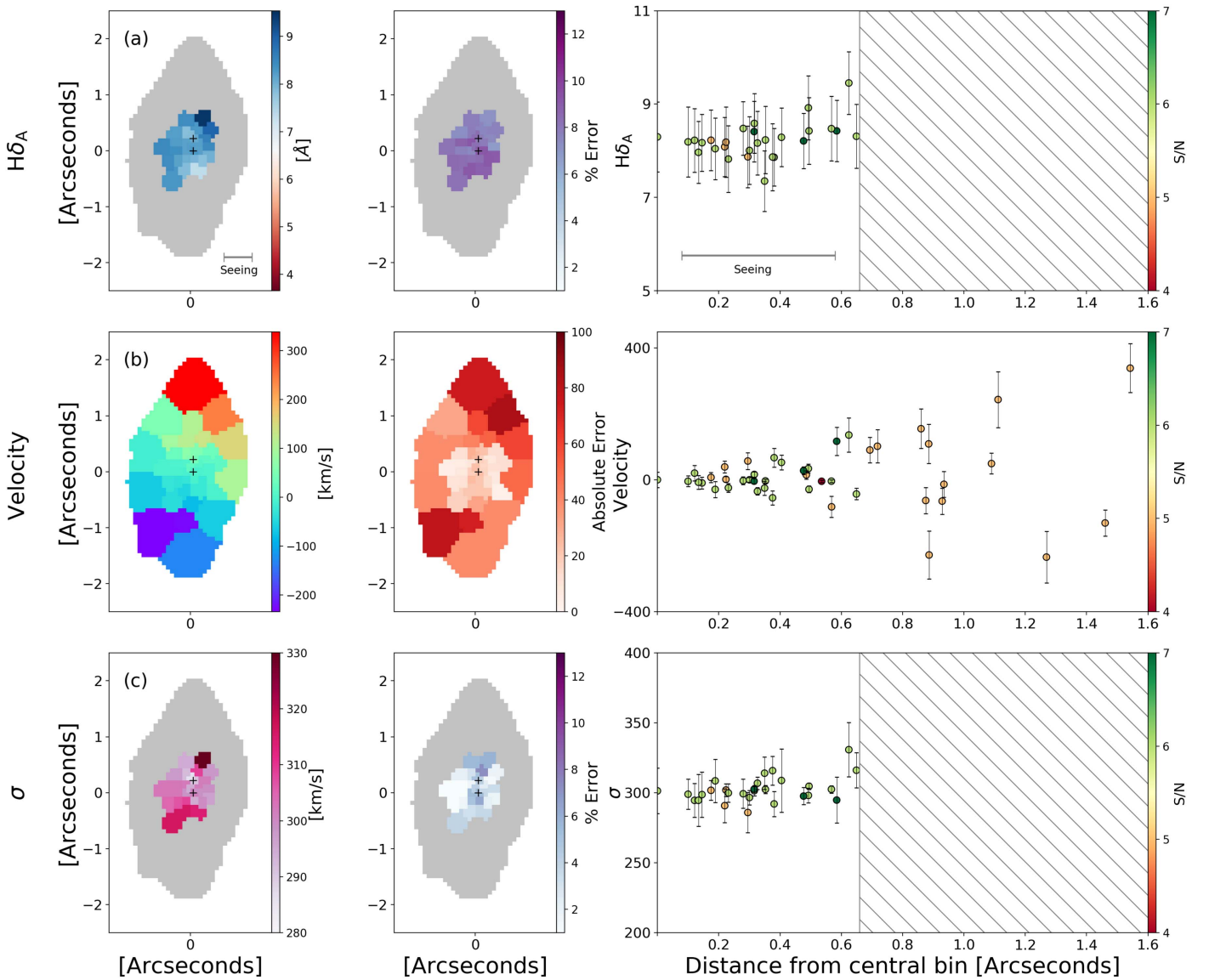


**Figure 2.** Stellar kinematic and spectral index maps. The two flux peaks are marked with black + symbols. The seeing is indicated with gray bars. The left column shows the measured values of the (a) equivalent width of  $H\delta_A$ , (b) velocity, and (c) velocity dispersion  $\sigma$  for each Voronoi bin. The middle column represents the estimated errors for each measurement. Velocity (row b) is measured with respect to the central bin, and its errors are presented as absolute values. The right column illustrates the relationship between the measured values and radial distance from the center of the galaxy. We omit outer bins below the target  $S/N = 6$  in rows (a) and (c). These bins are blocked out in gray in the left column and by gray hashed boxes in the right column.

$H\delta_A$  using the wide Worthey & Ottaviani (1997) bandpass definition, illustrated in Figure 1(b), with the `lick_ew` routine from the IDL `EZ_Ages` package written by G. Graves (Schiavon 2007; Graves & Schiavon 2008). The uncertainties are calculated via Monte Carlo resampling, as described in Section 2.1. The typical uncertainty in  $H\delta_A$  is  $\sim 0.7 \text{ \AA}$ .

The  $D_n4000$  index, which measures the strength of the 4000  $\text{\AA}$  break, is often used in conjunction with  $H\delta_A$  to probe the star formation history of galaxies (e.g., Poggianti & Barbaro 1997; Kauffmann et al. 2003; Kriek et al. 2011; Zahid et al. 2015; Zahid & Geller 2017). The feature is measured using only two bandpasses (Balogh et al. 1999) and is therefore highly sensitive to the flux calibration. In addition, as  $D_n4000$  is especially uncertain in the outer regions of our galaxy due to sky subtraction challenges, we use only the value of the central spatial bin to compare our analysis of SDSS J0912+1523 with previous work.

### 3. Results

Figure 2 shows the spectral index and stellar kinematics for each Voronoi bin as measured by `lick_ew` and `pPXF`. The left column represents our measurements of (a)  $H\delta_A$ , (b) velocity, and (c)  $\sigma$ . The colormap limits for  $H\delta_A$  were chosen to reflect that of the sample of  $z \sim 0.6$  PSBs discussed in Suess et al. (2017). The outer bins below  $S/N = 6$  are omitted from the  $H\delta_A$  and  $\sigma$  maps, as their low  $S/N$  makes them unreliable for measuring the EW and broadening of spectral features. We note that there exist a few central bins with  $S/N < 6$ , where the Voronoi process has failed to properly expand the bins. As these bins are small and have values consistent with the higher  $S/N$  regions, we have chosen to include them in our analysis. The middle column of Figure 2 gives the uncertainty of each value. For  $H\delta_A$  and  $\sigma$ , the uncertainty is given as a percentage error. Because all velocities are measured with respect to the central bin, the uncertainty in



the velocity is given as an absolute error. Finally, the right column shows the radial gradient of each property.

### 3.1. Spectral Indices

We measure a central  $H\delta_A$  of  $\sim 8.3 \text{ \AA}$  and  $D_n4000$  of  $\sim 1.18$ . Our measurements are in agreement with the spectral indices obtained from the SDSS data in Suess et al. (2017). These values place SDSS J0912+1523 at the boundary between typical starburst and post-starburst galaxy populations (Kauffmann et al. 2003; Suess et al. 2017). To ensure that SDSS J0912+1523 is indeed quenched, we search for the presence of star formation using  $[\text{O II}]\lambda 3727$  and  $[\text{O III}]\lambda 5007$ . Both emission lines are absent from our spectra, consistent with the low star formation rate (SFR) of  $2.1 \pm 0.8 M_\odot \text{ yr}^{-1}$  measured previously by Suess et al. (2017) using the line flux of the  $[\text{O II}]\lambda 3727$  doublet. SDSS J0912+1523, therefore, most likely represents a transitional object that has only just quenched.

$H\delta_A$ , as illustrated in Figure 2(a), appears flat in the inner  $\sim 0''.6$  region of the galaxy. In addition, we measure  $H\delta_A$  and  $D_n4000$  to be roughly the same for each of the peaks observed in Figure 1(a), which are marked with black + symbols in Figure 2. The reported  $\sim 0''.5$  seeing introduces some uncertainty as to whether we resolve the  $H\delta_A$  map. As we are able to resolve a  $\sim 0''.2$  asymmetry within the core, our seeing is likely a conservative estimate. We believe that the flatness of the  $H\delta_A$  (age) distribution is real, and that the two ‘‘cores’’ that we observe in Figure 1(a) likely share a common stellar population.

### 3.2. Kinematics

The stellar kinematics of SDSS J0912+1523 are illustrated by rows (b) and (c) in Figure 2, representing stellar velocity and  $\sigma$ , respectively. Due to beam smearing, the intrinsic velocity will likely be higher than we measure, while the intrinsic  $\sigma$  will be lower. The velocity field shows ordered rotation about the center of SDSS J0912+1523, while the  $\sigma$  field remains flat. The velocities at the positions of the two peaks are offset by  $\sim 40 \text{ km s}^{-1}$ , compared to the galaxy’s maximum velocity of  $338 \pm 74 \text{ km s}^{-1}$ . Considering the average uncertainty of  $22 \text{ km s}^{-1}$ , the offset is consistent with the velocity gradient with respect to the center of the galaxy. Based on the consistent velocity offset, lack of multiple  $\sigma$  peaks, and similar stellar populations, we assert that the two ‘‘cores’’ are part of the same galaxy and are rotating as a single object. They may be the remnants of a late-stage merger, or possibly a single core that is bisected by a dust lane. We note that the orientation of such a dust lane is not obviously consistent with the galaxy alignment and orientation.

We quantitatively compare the velocity and  $\sigma$  profiles in Figure 3(a). We measure a smooth velocity field for SDSS J0912+1523 from its 2D line-of-sight velocity distribution using `Kinometry` in IDL (Krajnović et al. 2006), represented by the green line. `Kinometry` allows us to account for possible changes in B/A as a function of redshift and gives velocities with smaller errors. The maximum velocity is  $242 \pm 17 \text{ km s}^{-1}$  at  $\sim 11 \text{ kpc}$ . The pPXF velocities along the galaxy’s major axis are marked in blue. Deviations from the smooth `Kinometry` model are consistent with the noise. Using the central velocity dispersion ( $\sigma$  of the central bin,  $\sigma_0$ ) and the rotational velocity measured from the `Kinometry` velocity profile at 5 kpc ( $V_5$ ),

we calculate rotational support ( $|V_5|/\sigma_0$ ). The 5 kpc physical parameter was chosen to match a sample of quiescent galaxies at  $0.6 < z < 1.0$  from the The Large Early Galaxy Census (LEGA-C) spectroscopic survey (van der Wel et al. 2016), shown in Figure 3(b) (Bezanson et al. 2018). Galaxies with high  $|V_5|/\sigma_0$  tend to be disk-like in morphology. At low  $|V_5|/\sigma_0$ , galaxies become pressure supported and exhibit spheroidal morphologies (Emsellem et al. 2007, 2011). For SDSS J0912+1523, we measure  $\sigma_0 = 301 \pm 16 \text{ km s}^{-1}$  and  $V_5 = 88 \pm 5 \text{ km s}^{-1}$ . Our estimate of rotational support is a lower limit, in part due to beam smearing, intrinsic inclination, and the limited radial range of our measurements. When measured at 10 kpc,  $V_{10} = 213 \pm 11 \text{ km s}^{-1}$ . These values indicate a retention of rotational support in the PSB.

We plot the rotational support of SDSS J0912+1523 against its stellar mass, as obtained by Suess et al. (2017), and compare them to the LEGA-C sample in Figure 3(b). Like our data, the LEGA-C observations (gray points) are spatially resolved and are not corrected for inclination or beam smearing. Bezanson et al. (2018) perform simulations of the LEGA-C observations with  $1''.0$  seeing using local quiescent galaxies from the Calar Alto Legacy Integral Field Area Survey (CALIFA) sample (blue solid line) and find that the measured  $|V_5|/\sigma_0$  values for the LEGA-C and CALIFA galaxies are likely underestimated by a factor of  $\sim 2.5$ . We plot the median  $|V_5|/\sigma_0$  of the LEGA-C galaxies per mass bin (red solid line) and adjust it by the underestimation factor to approximate the intrinsic relation for these quiescent galaxies at  $z \sim 0.8$  (red dashed line). We simulate the effects of beam smearing by a FWHM  $\sim 3.5 \text{ kpc}$  (corresponding to  $\sim 0''.5$  at this redshift) on the CALIFA data cubes and estimate that our measured  $|V_5|/\sigma_0$  of SDSS J0912+1523 (green star) will underestimate the intrinsic value by a factor of  $\sim 1.3$ , which we indicate by the green arrow.

The LEGA-C sample reveals a correlation between mass and rotational support, consistent with observations of the nearby universe (Emsellem et al. 2011). There is a significant increase in pressure support at  $\log M_*/M_\odot > 11.2$ , above which SDSS J0912+1523 falls. Our target PSB is *at least* consistent with typical quiescent galaxies at similar redshift as probed by LEGA-C, which exhibit stronger rotational support than the nearby CALIFA galaxies of similar mass. We note, however, that beam smearing can only move our galaxy toward higher rotation.

Finally, we compare the stellar and molecular gas components of SDSS J0912+1523. Recent ALMA observations of SDSS J0912+1523 by Suess et al. (2017) uncovered a substantial amount of cold gas:  $M_{\text{gas}} = (3.4 \pm 0.2) \times 10^{10} M_\odot$ , corresponding to a gas fraction of  $\sim 30\%$ . We plot the velocity field of the molecular gas, as traced by CO(2–1), beside the stellar velocity field in Figure 4. With a spatial resolution of  $1''.7 \times 2''.4$ , we do not know the spatial distribution of gas. However, based on the similar amplitudes and rotation, we determine that the gas and stars are likely aligned.

## 4. Discussion and Conclusions

Through kinematic and spectroscopic analysis of SDSS J0912+1523 using optical IFU data obtained with Gemini, in conjunction with the analysis of ALMA data first presented in Suess et al. (2017), we determine that the massive  $z \sim 0.7$  galaxy:

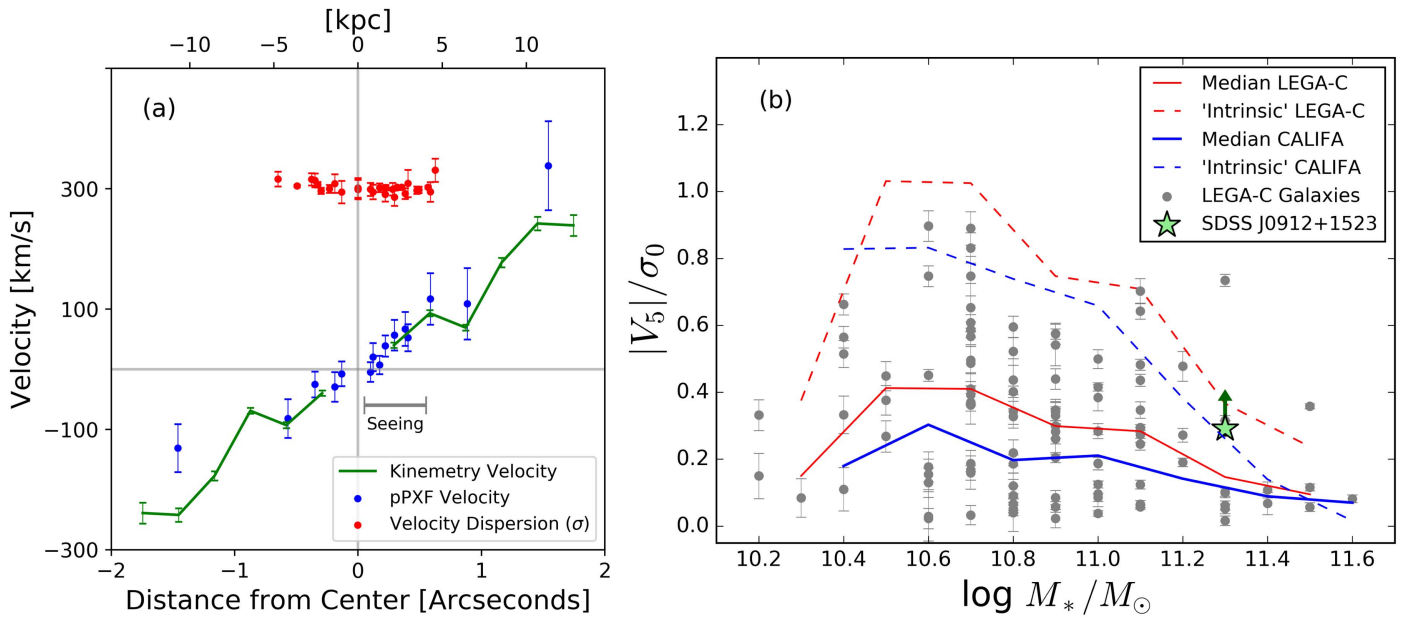


**Figure 3.** (a) Velocity and velocity dispersion of the SDSS J0912+1523 Voronoi bins as a function of distance from the center. (b) Rotational support at 5 kpc vs. stellar mass of SDSS J0912+1523, compared to similar-redshift quiescent galaxies from the LEGA-C survey and local galaxies from the Calar Alto Legacy Integral Field Area Survey (CALIFA; Bezanson et al. 2018). The median observed rotational support of the LEGA-C and CALIFA galaxies per mass bin are plotted in red and blue, respectively, with dashed lines reflecting intrinsic values. The intrinsic rotational support of the LEGA-C sample and SDSS J0912+1523 (indicated by the green arrow) are simulated with using the CALIFA sample. SDSS J0912+1523 is roughly consistent with the typical, similar-mass LEGA-C galaxy and is more rotationally supported than local CALIFA galaxies.

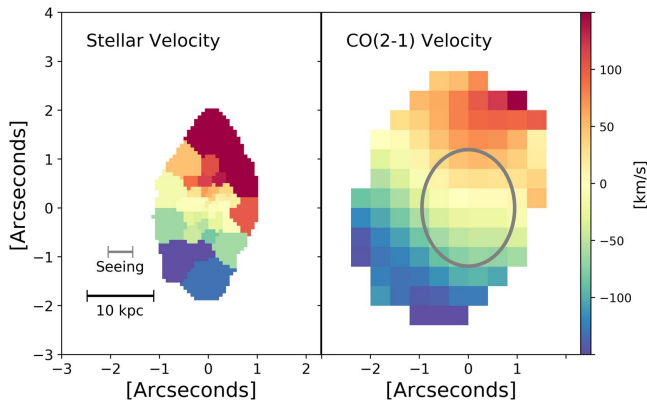


**Figure 4.** Stellar and cold molecular gas velocity fields of SDSS J0912+1523, as observed by Gemini and ALMA. The stellar seeing and ALMA beam are indicated in gray. The motion of the cold molecular gas is consistent with the stellar component.

1. is a young PSB that has effectively quenched its star formation;
2. may contain either two cores or a dust lane that bisects a single core;
3. has no detectable age gradient within 5 kpc of its center, within the constraints of the seeing;
4. maintains significant rotational support compared to similar-mass quiescent galaxies;
5. contains an unusually large cold gas fraction for its apparent SFR; and
6. maintains ordered gas rotation that roughly matches the stellar component, with no evidence of significant outflow.

We now compare the characteristics of SDSS J0912+1523 to predictions from the most common quenching scenarios for massive quiescent galaxies. In particular, we focus on: mergers, compaction, outflows, and morphological quenching.

Based on our observations, none of these scenarios seem to accurately predict all of the characteristics of our target PSB. The significant rotational support and regular velocity field are most consistent with both gas-rich merger and compaction models, while they are inconsistent with the dispersion-dominated systems that result from gas-poor mergers (Emsellem et al. 2007). The abundance of cold molecular gas within SDSS J0912+1523, on the other hand, suggests that neither depletion nor heating of gas led to its quenching, which limits the role of compaction and gas-rich major mergers as the main drivers of star formation suppression. The high gas fraction is more consistent with gas-rich *minor* mergers and morphological quenching. However, it is unclear whether SDSS J0912+1523 contains *too much* gas and rotation for morphological quenching to be viable (Martig et al. 2009). The alignment of the gas and stellar velocity fields argue against an external origin for the gas, and there is no evidence for strong molecular gas outflows in the ALMA data. Further constraints arise from the spectral indices and lack of emission lines in the galaxy’s spectra. Evidence of a recent starburst is consistent with compaction, though the apparent lack of a radial age gradient may indicate otherwise. It is not clear whether a gas-rich minor merger could fuel a starburst at our redshift: gas-rich minor merger models are typically done at low redshifts, so the application of these models may not be straightforward at  $z \sim 0.7$ , where the gas fraction is higher (van de Voort et al. 2018).

Whatever process quenched SDSS J0912+1523 must allow it to retain both a large gas fraction and significant rotational support. To definitively constrain the scenarios beyond this,

more data are required. Radio or X-ray observations may reveal the presence of quasar activity, while deeper IR and radio observations, as with the Very Large Array (VLA), may uncover heavily dust-obscured star formation. Information about the dark matter halo and its environment is also vital, as many quenching models make halo predictions, and the environment in which quiescent galaxies develop may influence their formation histories (Zabludoff et al. 1996; Zolotov et al. 2015). *Hubble Space Telescope* (HST) imaging and higher-resolution gas observations could greatly improve our understanding of SDSS J0912+1523 by revealing its morphology: whether it is bulge-dominated or disk, how the gas is distributed, whether there are weak outflows, the nature of the “cores,” and whether mergers greatly influence the galaxy’s behavior. In the meantime, expanding our analysis to include other PSBs may help determine whether SDSS J0912+1523 is a special case, or whether a majority of PSBs—and possibly quiescent galaxies as a whole—quench via a similar process.

We wish to thank Charlie Conroy for sharing the stellar population synthesis model templates with us. We also sincerely thank Michael Strauss, Marijn Franx, and Khalil Hall-Hooper for their help, comments, and support.


This paper is based on observations obtained at the Gemini Observatory, acquired through the Gemini Observatory Archive under Program ID GN-2016A-FT-6 and processed using the Gemini IRAF package, which is operated by the Association of Universities for Research in Astronomy, Inc., under a cooperative agreement with the NSF on behalf of the Gemini partnership: the National Science Foundation (United States), the National Research Council (Canada), CONICYT (Chile), Ministerio de Ciencia, Tecnología e Innovación Productiva (Argentina), and Ministério da Ciência, Tecnologia e Inovação (Brazil).

This paper makes use of the following ALMA data: ADS/JAO.ALMA#2016.1.00126.S. ALMA is a partnership of ESO (representing its member states), NSF (USA) and NINS (Japan), together with NRC (Canada), NSC and ASIAA (Taiwan), and KASI (Republic of Korea), in cooperation with the Republic of Chile. The Joint ALMA Observatory is operated by ESO, AUI/NRAO and NAOJ. The National Radio Astronomy Observatory is a facility of the National Science Foundation operated under cooperative agreement by Associated Universities, Inc. This material is based upon work supported by the National Science Foundation Graduate Research Fellowship Program under grant No. DGE 1106400.

D.N. was funded in part by NSF AST-1715206 and HST AR-15043.0001.

#### ORCID iDs

Justin S. Spilker  <https://orcid.org/0000-0003-3256-5615>  
Katherine A. Suess  <https://orcid.org/0000-0002-1714-1905>

Mariska Kriek  <https://orcid.org/0000-0002-7613-9872>  
Desika Narayanan  <https://orcid.org/0000-0002-7064-4309>  
Robert Feldmann  <https://orcid.org/0000-0002-1109-1919>  
Arjen van der Wel  <https://orcid.org/0000-0002-5027-0135>  
Petchara Pattarakijwanich  <https://orcid.org/0000-0001-8451-5316>

#### References

- Alam, S., Albareti, F. D., Prieto, C. A., et al. 2015, *ApJS*, 219, 12  
Alatalo, K., Cales, S. L., Appleton, P. N., et al. 2014, *ApJL*, 794, L13  
Balogh, M. L., Morris, S. L., Yee, H. K., et al. 1999, *ApJ*, 527, 54  
Bell, E. F., Wolf, C., Meisenheimer, K., et al. 2004, *ApJ*, 608, 752  
Bezanson, R., van der Wel, A., Pacifici, C., et al. 2018, arXiv:1804.02402v1  
Cananzi, K., Augarde, R., & Legueux, J. 1993, *A&AS*, 101, 599  
Cappellari, M. 2017, *MNRAS*, 466, 798  
Cappellari, M., & Copin, Y. 2003, *MNRAS*, 342, 345  
Cappellari, M., & Emsellem, E. 2004, *ASP*, 116, 138  
Carollo, C. M., Bschorr, T. J., Renzini, A., et al. 2013, *ApJ*, 773, 112  
Cenarro, A. J., & Trujillo, I. 2009, *ApJL*, 696, L43  
Dekel, A., & Burkert, A. 2014, *MNRAS*, 438, 1870  
Emsellem, E., Cappellari, M., Krajnović, C., et al. 2007, *MNRAS*, 379, 401  
Emsellem, E., Cappellari, M., Krajnović, C., et al. 2011, *MNRAS*, 414, 888  
Faber, S. M., Willmer, N. A., Wolf, C., et al. 2007, *ApJ*, 665, 265  
Goto, T., Nichol, R. C., Okamura, S., et al. 2003, *PASJ*, 55, 771  
Graves, G. J., & Schiavon, R. P. 2008, *ApJS*, 177, 2  
Hopkins, P. F., Cox, T. J., Hernquist, L., et al. 2009, *ApJ*, 691, 1424  
Hopkins, P. F., Cox, T. J., Kereš, D., & Hernquist, L. 2008, *ApJS*, 175, 390  
Johansson, P. H., Naab, T., & Ostriker, J. P. 2009, *ApJL*, 697, L38  
Kauffmann, G., Heckman, T. M., White, S. D. M., et al. 2003, *MNRAS*, 341, 54  
Krajnović, D., Cappellari, M., de Zeeuw, P. T., & Copin, Y. 2006, *MNRAS*, 366, 787  
Kriek, M., Labbé, I., Conroy, C., et al. 2010, *ApJL*, 722, L64  
Kriek, M., van Dokkum, P. G., Whitaker, K. E., et al. 2011, *ApJ*, 743, 2  
Labbé, I., Huang, J., Franx, M., et al. 2005, *ApJL*, 624, L81  
Le Borgne, D., Abraham, R., Daniel, K., et al. 2006, *ApJ*, 642, 48  
Lena, D. 2014, arXiv:1409.8264  
Mao, S. A., & Ostriker, E. 2018, arXiv:1801.06544  
Martig, M., Bournaud, F., Teyssier, R., & Dekel, A. 2009, *ApJ*, 707, 250  
Naab, T., Johansson, P. H., & Ostriker, J. P. 2009, arXiv:0903.1636v4  
Newman, A. B., Belli, S., & Ellis, R. S. 2015, *ApJL*, 813, L7  
Pattarakijwanich, P., Strauss, M. A., Ho, S., & Ross, N. 2016, *ApJ*, 883, 19  
Poggianti, B. M., & Barbaro, G. 1997, *A&A*, 325, 1030  
Pontzen, A., Tremmel, M., Ross, N., et al. 2017, *MNRAS*, 465, 547  
Schiavon, R. P. 2007, *ApJS*, 171, 146  
Sell, P. H., Tremonti, C. A., Hickox, R. C., et al. 2014, *MNRAS*, 441, 3417  
Strateva, I., Ivezić, Ž., Knapp, G. R., et al. 2001, *AJ*, 122, 1861  
Suess, K., Bezanson, R., Spilker, J., et al. 2017, *ApJL*, 846, L14  
Tacchella, S., Carollo, C. M., Renzini, A., et al. 2015, *Sci*, 348, 6232  
Tremonti, C. A., Moustakas, J., & Diamond-Stanic, A. M. 2007, *ApJS*, 663, L77  
van de Voort, F., Davis, T. A., Matsushita, S., et al. 2018, arXiv:1801.08140  
van der Wel, A., Noeske, K., Bezanson, R., et al. 2016, *ApJS*, 223, 29  
Wellons, S., Torrey, P., Ma, C. P., et al. 2015, *MNRAS*, 449, 361  
Worthey, G., & Ottaviani, D. L. 1997, *ApJS*, 11, 377  
Yano, M., Kriek, M., van der Wel, A., & Whitaker, K. 2016, *ApJL*, 817, L21  
Zabludoff, A. I., Zaritsky, D., Lin, H., et al. 1996, *ApJ*, 466, 104  
Zahid, H. J., Damjanov, I., Geller, M. J., & Chilingarian, I. 2015, *ApJ*, 806, 122  
Zahid, H. J., & Geller, M. J. 2017, arXiv:1701.01350v3  
Zolotov, A., Dekel, A., Madelkre, N., et al. 2015, *MNRAS*, 450, 2327